# Polarization Effects in Semiconductors

## From Ab InitioTheory to Device Applications

Colin Wood • Debdeep Jena
Editors

# Polarization Effects in Semiconductors

## From Ab InitioTheory to Device Applications

Springer

Colin Wood
US Office of Naval Research
Arlington, VA
USA

Debdeep Jena
University of Notre Dame
Notre Dame, IN
USA

Library of Congress Control Number: 2007932418

ISBN 978-0-387-36831-3 e-ISBN 978-0-387- 68319-5

Printed on acid-free paper.



9 8 7 6 5 4 3 2 1

springer.com

# Preface

In the last two decades basic semiconductor research has increasingly focussed attention away from cubic crystal III-V and II-VI compounds toward the "wide-bandgap semiconductors" Ga, Al, In binary and ternary nitrides, and silicon carbide. These smaller anion compounds pack more densely in hexagonal crystals, with the consequence of very high spontaneous and deformation induced electrostatic polarization.

The importance and potential functionality of was rapidly recognized in the late 1990s. In 2000 the Multi-disciplinary University Research Initiative (MURI) of "Polarization Effects in Wide Bandgap Semiconductors" was initiated by the Office of Naval Research to accelerate and consolidate understanding, engineering and device application of the extra electro-physical parameter space. The winning program, "Polaris" by teams centered at UC San Diego, and Cornell University, was one of the most productive in the history of the MURI program, and is testament to the value of sponsored collaborative research so ardently defended by the Director of Defense Research and Engineering (DDR&E) Office of the Secretary of Defense (OSD).

Electronic polarization has profound consequences on the electrostatics and electrodynamics of epitaxial films and heterostructures. Polaris team members developed a comprehensive scientific understanding and made many conceptual advances in polarization-related semiconductor physics. As a result, many electronic and optical devices have been significantly improved and novel devices conceived and realized.

This book is an attempt to ensure that the pioneering advances of the Polaris investigators are collected and expanded to allow efficient recognition and understanding of the many new scientific and engineering principles, considerations and applications developed in the 5 year program.

Each chapter addresses aspects of polarization effects from a different perspective, and for different purposes. There is some overlap in the introductory content in several chapters, albeit each with its own unique flavor. The editors decided to retain this format as it serves to make each chapter self-contained, so that readers

have the option of perusing them independently without loss of continuity, and to guide readers more effectively to the subtle differences in perspectives.

Arlington, VA *Colin Wood*
Notre Dame, IN *Debdeep Jena*

# Contributors

P. Alpay
Materials Science and Engineering Program & Institute of Materials Sciences, University of Connecticut, Storrs, CT 06269 USA, e-mail: p.alpay@ims.uconn.edu

O. Ambacher
Institute of Micro- and Nanotechnologies, Technical University Ilmenau, D-98693 Ilmenau, Germany, e-mail: oliver.ambacher@tu-ilmenau.de

P. M. Asbeck
Department of Electrical and Computer Engineering, University of California, San Diego, CA 92093 USA, e-mail: asbeck@ece.ucsd.edu

J. Bernholc
Center for High Performance Simulation & Department of Physics, North Carolina State University, Raleigh, NC 27695, USA, e-mail: bernholc@ncsu.edu

P. Boguslawski
Institue of Physics, Polish Academy of Sciences, Al. Lotnikow 32/46, 02-668 Warsaw, Poland, e-mail: bogus@ifpan.edu.pl

R. Butté
Laboratory of Advanced Semiconductors for Photonics and Electronics (LASPE), EPFL, Station 3, CH-1015, Lausanne, Switzerland, e-mail: raphael.butte@epfl.ch

M. V. S. Chandrashekhar
Electrical and Computer Engineering, Cornell University, Ithaca, NY 14853, USA, e-mail: mc296@cornell.edu

V. Cimalla
Institute of Micro- and Nanotechnologies, Technical University Ilmenau, D-98693 Ilmenau, Germany, e-mail: volker.cimalla@tu-ilmenau.de

N. Grandjean
Laboratory of Advanced Semiconductors for Photonics and Electronics (LASPE),

EPFL, Station 3, CH-1015, Lausanne, Switzerland,
e-mail: nicolas.grandjean@epfl.ch

D. Jena
Department of Electrical Engineering, University of Notre Dame, Notre Dame, IN 46556 USA, e-mail: djena@nd.edu

G. Koley
Department of Electrical Engineering, University of South Carolina, Columbia, SC 29208, USA, e-mail: koley@engr.sc.edu

J. Leach
Department of Electrical and Computer Engineering, Virginia Commonwealth University, Richmond, VA 23284, USA, e-mail: s2jleach@vcu.edu

J. Mantese
United Technologies Research Center, 411 Silver Lane, MS 129-45, East Hartford, CT 06108, USA, e-mail: mantesjv@utrc.utc.com

H. Morkoç
Department of Electrical and Computer Engineering, Virginia Commonwealth University, Richmond, VA 23284, USA, e-mail: hmorkoc@vcu.edu

J. Singh
Electrical Engineering and Computer Science Dept. University of Michigan, Ann Arbor, MI 48109, USA, e-mail: singh@engin.umich.edu

M. Singh
Electrical Engineering and Computer Science Dept. University of Michigan, Ann Arbor, MI 48109, USA, e-mail: msingh@eecs.umich.edu

M. G. Spencer
Electrical and Computer Engineering Dept. Cornell University, Ithaca, NY 14853, USA, e-mail: spencer@ece.cornell.edu

C. I. Thomas
Electrical and Computer Engineering Dept. Cornell University, Ithaca, NY 14853, USA, e-mail: cit5@cornell.edu

Y.-R. Wu
Assistant Professor, National Taiwan University, Graduate Institute of Photonics and Optoelectronics and Department of Electrical Engineering, MD 617, No 1. Roosevelt Road Sec. 4, Taipei 10617, Taiwan, e-mail: yrwu@cc.ee.ntu.edu.tw

E. T. Yu
Electrical and Computer Engineering Dept. University of California, San Diego, CA 92093 USA e-mail: ety@ece.ucsd.edu

# Contents

# Theoretical Approach to Polarization Effects in Semiconductors

Piotr Boguslawski and J. Bernholc

## 1 Introduction

As a rule, investigations of physical effects in solids are motivated by the need of understanding at a fundamental level, which facilitates their effective application in the fabrication of devices. The problem of electrical polarization of piezoelectric, ferroelectric, and pyroelectric solids is no exception. In the last 15 years we have witnessed very intensive investigations of the theory of spontaneous polarization, as well as of the dielectric response of crystals to external perturbations. Our current understanding stems from the development of electronic structure calculations based on first principles, and subsequently from evolution of appropriate theoretical approaches allowing for both a proper definition of polarization and accurate calculations. From the experimental side, much of the impetus came from experimental work devoted to, e.g., GaN-like group-III nitrides, in which internal electric fields of both pyro- and piezoelectric origin are large, determining the properties of quantum structures and devices [1]. Spectacular progress in this area has led to innovative devices described in several chapters of this book.

There are two important issues clarified by first principles calculations in the last two decades. The first achievement was to provide a link between *microscopic* distribution of electrons determined by first-principles calculations and the description based on classical *macroscopic* electrostatics. In particular, calculations have shown how actual charge densities and dipole layers at surfaces and/or interfaces in semiconductor heterostructures look like at the atomic scale, what are their localization and origin, etc. These basic concepts and ingredients of classical electrodynamics developed during the last two centuries are now visualized by first principles theory. Typical results are described in Sections 6 and 7.

The second success is a demonstration of the fact that spontaneous polarization and piezoelectric effects are bulk properties of solids, and thus may be studied by calculations performed for infinite crystals [2, 3]. This subject was first treated in the paper by Martin [4], who showed that the piezoelectric tensor of an insulator is a bulk quantity. In fact, the development of elegant theoretical approaches

[2, 3] has enabled efficient calculations, and the results are in good agreement with experiment. Furthermore, a wealth of new information has been obtained. In this chapter, we briefly summarize the theoretical approaches and illustrate them with appropriate examples.

As an example of the role played by the electric field, we discuss field-induced electromigration of hydrogen in GaN/AlN heterojunctions rather than the impact of electric field on the electronic structure, which was discussed at length in many papers [1] and other chapters of this book.

## 2 Basic Electrostatics

The distribution of free carriers and the magnitude of electric currents in a semiconductor are determined by electric fields. In a "classical" semiconductor or semiconductor structure, such as a Si-based junction, the field is of external origin. The electric field inside the structure is determined by, e.g., the applied voltage, which is screened by electrons and nuclei of the solid. The situation is more complex in ferroelectrics, pyroelectrics, and piezoelectrics, where there may exist an internal field even in the absence of the external one, due to the presence of non-vanishing electric polarization. Independent of the origin of the fields, electrostatics of macroscopic media introduce basic concepts and relationships briefly recalled below.

In a bulk homogeneous insulator, the electric field $\boldsymbol{E}$, polarization $\boldsymbol{P}$, and the electric displacement $\boldsymbol{D}$ are related by:

$$\boldsymbol{D} = \varepsilon \boldsymbol{E} = \boldsymbol{E} + 4\pi \boldsymbol{P}, \tag{1}$$

see the classical textbook by Jackson [5]. Here $\varepsilon$ is the static dielectric constant. According to Poisson's equation, $\boldsymbol{D}$ is determined by the external electric charge density $qn$:

$$\mathrm{div}\boldsymbol{D} = 4\pi\, qn\, (\mathbf{r}), \tag{2}$$

where $q$ is the elementary (positive) charge. To solve this equation one needs boundary conditions. For a finite solid, boundary conditions at surfaces or at interfaces between layers of a heterostructure play an important role, since they determine discontinuities at the boundaries and thus the magnitudes of fields in the whole system. The continuity condition at the surface reads [5]

$$\Delta \boldsymbol{D} \bullet \mathbf{i} = 4\pi\, \sigma. \tag{3}$$

Here, $\Delta \boldsymbol{D} = \boldsymbol{D}_2 - \boldsymbol{D}_1$, where $\boldsymbol{D}_2$ is outside and $\boldsymbol{D}_1$ inside the solid, and $\mathbf{i}$ is the unit vector normal to the surface. Thus, the change in the normal component of the displacement is determined by the surface charge density $\sigma$. It should be stressed that $\sigma$ is of *external* origin, as it follows from the Poisson's equation, Eq. 2, and does not include polarization charges. For example, $\sigma$ can be the macroscopic charge density on the plates of a charged capacitor, which generates the electric field. Discontinuity

of polarization at the surface or, in general, at an interface between two dielectrics, is related to the polarization surface charge density $\sigma_{pol}$ by

$$-\Delta \boldsymbol{P} \bullet \mathbf{i} = \sigma_{pol} \tag{4}$$

Eqs. 3–4 indicate that the field in the *bulk* of an insulator is defined by the *surface* charge. This is the basis of operation of sensors, where the adsorption of a molecule changes the electric characteristics of a device. Moreover, Eqs. 3–4 show that in the absence of external charges at interfaces of, e.g., a superlattice, discontinuities of the field and the polarization are related by $\Delta \boldsymbol{E} \bullet \mathbf{i} = -4\pi\, \Delta \boldsymbol{P} \bullet \mathbf{i}$.

Similarly, the discontinuity of the electrostatic potential $\phi$ is determined by the dipole layer at the surface (or interface). In analogy with Eq. 3, the discontinuity of the electrostatic potential is given by

$$\Delta\, \phi = 4\pi\, \delta, \tag{5}$$

where $\delta$ is the surface dipole density. Clearly, as already indicated, the continuity equations apply both to free surfaces and to interfaces in heterostructures and superlattices. Both are of interest in this review.

To highlight the difference between the situations relevant for the discussions that follow, we show in Fig. 1 three cases of an insulator with and without surface charges. In the first case, two opposite surfaces are charged. This situation holds for a solid placed in a charged capacitor. The surface charge densities are of external origin (capacitor plates), and they induce a non-vanishing displacement field $\boldsymbol{D}$ in the solid in which polarization $\boldsymbol{P}$ and electric field $\boldsymbol{E}$ are parallel. The polarization induced by the external electric field consists of a relative displacement of positive and negative charges inside a solid, which screen (weaken) these fields.

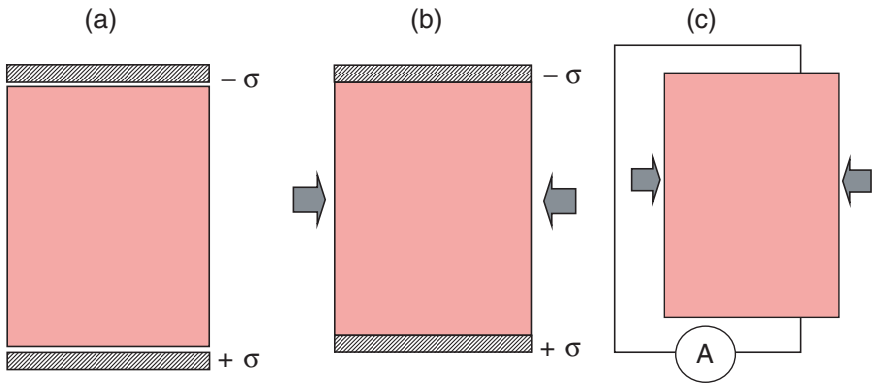


**Fig. 1** Surface charges of opposite sign, shown as gray layers, produced by (a) external reservoirs, (b) the piezoelectric effect, with the gray arrows indicating the external pressure, and (c) a strained solid shown in (b) but with short-circuited surfaces, which led to a flow of a current. The configurations shown in (b) and (c) corresponds to, e.g., a zinc-blende crystal strained uniaxially in the [110] direction, which induces polarization oriented in the [001] direction.

The second case looks similar, but now the surface charges are obtained when a piezoelectric is appropriately strained. In this case there is no external charge, thus $\boldsymbol{D} = 0, \boldsymbol{E} = -4\pi \boldsymbol{P}$, i.e., $\boldsymbol{P}$ and $\boldsymbol{E}$ are antiparallel. The surface charge density owns its origin to bulk piezoelectric polarization. By applying stress that produces polarization, an internal electric current is induced, leading to the separation of charge and formation of charged surface layers. The fact that polarization is related to current flow is exploited in the modern approach to theory of polarization, briefly summarized in Sec. 5.

Finally, in the case of a strained piezoelectric, the electric field may be eliminated by short-circuiting the two charged surfaces (i.e., $\boldsymbol{E} = 0$, but $\boldsymbol{P} \neq 0$ and $\boldsymbol{D} = 4\pi \boldsymbol{P}$). This case is of interest for the calculations of polarization presented below, which explicitly assume a vanishing electric field. The strain-induced electric field explains the difference between longitudinal and transverse optical phonons in a polar semiconductor like GaAs: in the former case phonon-induced atomic displacements induce not only the polarization, but also an electric field of opposite sign, which provides an additional restoring force that increases the frequency of the longitudinal phonon relative to the transverse branch.

## 3 Polarization

In general, polarization of a solid in a finite electric field may be expressed as a sum

$$\boldsymbol{P} = \boldsymbol{P}_0 + \boldsymbol{P}_{el} + \boldsymbol{P}_{lat}, \tag{6}$$

where $\boldsymbol{P}_0$ is the spontaneous polarization of the lattice at equilibrium and zero electric field, while $\boldsymbol{P}_{el}$ and $\boldsymbol{P}_{lat}$ correspond to the electron and lattice contributions. The low symmetry of several types of lattices allows the presence of non-vanishing bulk polarization at zero field. In particular, a crystal with the Wurtzite structure is pyroelectric, and its polarization is oriented parallel to the [0001] direction, i.e., only along the *c*-axis. It is always present and has the same sign independently of the field. In contrast, in ferroelectrics such as the Perovskites, the orientation of polarization can be reversed by an external electric field. In real samples, the intrinsic polarization is in general screened by free carriers that originate from ionized native defects present in the bulk of the sample, and/or by surface charges.

In the regime of linear response, the two latter components of Eq. (6), which are induced by either electric field or stress, may be expressed as follows. $\boldsymbol{P}_{el}$ is the electronic screening obtained under the condition that the atoms are not displaced from their equilibrium sites,

$$\boldsymbol{P}_{el} = (1/4\pi)(\varepsilon_\infty - 1)\boldsymbol{E}, \tag{7}$$

where $\varepsilon_\infty$ is the electron component of the dielectric tensor, i.e., the high-frequency dielectric constant describing the response of the electron gas at frequencies higher than the phonon frequencies, but lower than electronic excitations. The full dielectric

response to an external electric field, given by the static dielectric constant introduced in Eq. 1, includes also the lattice contribution, i.e., possible displacements of the nuclei from their equilibrium positions.

$\boldsymbol{P}_{lat}$ is induced by the lattice response and describes the piezoelectric effect, i.e., lattice polarization in vanishing electric field. The stress-induced polarization consists of two terms:

$$\boldsymbol{P}_{lat} = (q/\Omega)Z^*\boldsymbol{u} + \kappa\,\mathbf{e}. \tag{8}$$

The first is given by the relative displacements of sublattices in ionic crystals. The ionic displacements $\boldsymbol{u}_i$ relative to the cell center satisfy $\Sigma\boldsymbol{u}_i = 0$. For example, in the zinc blende structure the relative displacement $\boldsymbol{u}$ of cation and anion sublattices change the dipole moment of the unit cell by $Z^*\boldsymbol{u}$, where $Z^*$ is the Born effective charge and $\Omega$ is the unit cell volume. The second term describes polarization induced by strain when the sublattices are not displaced relative to each other, i.e., the atomic coordinates are rescaled by the macroscopic stress, but the electrons are allowed to relax due to the stress-induced changes in distances between atoms. $\kappa$ is the so-called clamped-ion component of the piezoelectric tensor, and $\mathbf{e}$ is the strain field tensor.

Finally, it is important to observe that the quantity accessible experimentally is not the polarization itself, but rather its changes induced by temperature changes (pyroelectricity), by external pressure (piezoelectricity), or electric field [3]. Similarly, as will be described below, in theoretical calculations polarization of a system is defined and calculated with respect to a non-polar phase.

Before presenting the recently developed advanced theory we illustrate in the next section the basic concepts underlying the macroscopic Eqs. (1–5) with examples of results obtained by microscopic *ab initio* calculations.

## 4 *Ab Initio* Calculations of the Electronic Structure

From the theoretical point of view, electrostatics of solids poses a question of how to compute the response of a dielectric to two most important external perturbations, i.e., the electric field and pressure. The electric field in a material is determined by the distribution of atoms and their electrons. To support an electric field the material must be an insulator, otherwise the field would be screened by electrons. Calculations of the vibronic, dielectric, piezoelectric, and ferroelectric properties based on density functional perturbation theory are described in Ref. [6]. An alternative approach involving analysis of electron redistribution and the phases of electron wavefunctions leads to a relatively simple, intuitive description of polar materials. It is presented briefly in the next Section. In both cases, the starting point is provided by *ab initio* calculations of the electronic structure based on the density functional theory (DFT).

For a given configuration of atoms, DFT [7] accurately predicts the distribution of electrons through the solution of Schrödinger-like Kohn-Sham equations for the

one-electron wave functions $\psi_i$ (in Rydbergs):

$$\left\{-\nabla^2 + V_N(\vec{r}) + \int \frac{2\rho(\vec{r}')d\vec{r}'}{|\vec{r}-\vec{r}'|} + \mu_{xc}[\rho(\vec{r})]\right\}\psi_i(\vec{r}) = \varepsilon_i\psi_i(\vec{r}), \quad i = 1,\ldots M. \quad (9)$$

Here, the first term represents the kinetic energy, the second is the potential due to nuclei (or atomic cores in the pseudopotential approach), the third is the classical electron-electron repulsion potential, and the fourth, the so-called exchange and correlation potential, accounts for the Pauli principle and spin effects. Summing over squares of the $M$ occupied wave functions gives the microscopic electron density $\rho$.

Semiconductors of interest for this chapter contain either 2 atoms in the unit cell (GaAs or GaN in the zinc-blende (*zb*) phase) or 4 (GaN and AlN in the Wurtzite (*w*) structure). More complex materials, including those containing defects or surfaces, can be modeled with a large, periodically-repeated unit cell, containing tens or hundreds of atoms. This is also the case for superlattices. The methods for solving DFT equations for perfect crystals or large "supercells" are by now quite advanced and several techniques exist for obtaining the wave functions and optimizing the structural parameters of a material by minimizing the total energy of the system [8]. For example, the methods that we use employ real-space grids and multi-grid acceleration techniques [9]. The use of grids leads to effective parallelization over hundreds of processors through domain decomposition, thereby enabling accurate calculations for rather large supercells.

## 5 Modern Theory of Polarization

The polarization of a solid can be expressed as a sum of ionic and electronic contributions

$$\vec{P} = \vec{P}_{ion} + \vec{P}_{el} = \frac{q}{V_{sample}}\left[\sum_l Z_l\vec{b}_l - \int\limits_{sample} \vec{r}\rho(\vec{r})d\vec{r}\right] \quad (10)$$

where $Z_l$ and $\vec{b}_l$ are the ionic charge and position of the $l$-th atom in the solid, $\rho(\vec{r})$ is the electron density, and $V_{sample}$ is the volume of the sample. In the pseudopotential approach, $Z_l$ is the charge of the ionic core and only valence electrons are taken into account. However, calculations directly based on this definition were never performed for at least two reasons. First, a straightforward summation over charges would need to include the entire sample and its surfaces, which is prohibitively expensive in terms of computational time. The second and more important reason that motivated an impressive theoretical effort in the last two decades is the following. It is empirically known that polarization (or rather polarization changes, which are actually measured, see Sec. 3) is a bulk property, and therefore independent of the state of surface of the sample, its reconstruction, etc. The bulk nature of polarization

of a piezoelectric insulator was first demonstrated by Martin [4]. However, the calculations for bulk systems use periodic unit cells; there are no surfaces and the field must be zero in order to satisfy the periodic boundary conditions. Furthermore, different unit cells can be used to describe a periodic structure and different cells cut through different bonds. A calculation of a dipole moment thus turns out to give different values, depending on what unit cell is used. Only for the case of well-localized electrons, *e.g.*, for negative ions, is the dipole moment per unit cell uniquely defined. This is the well-known Clausius-Mossotti limit, used to relate the dielectric constant to atomic polarizabilities in ionic solids.

It was also recognized that polarization of an infinite crystal is not a uniquely-defined quantity [10] and is in fact multi-valued [11]. Consequently, the physical quantity that is to be evaluated is the *difference* between macroscopic polarizations of a solid in two different states. Typically, one of these states is a non-polar reference state. This approach enables calculations for infinite crystals, where surface effects are absent by construction. Furthermore, comparisons between the polar and non-polar states often provide deep insight into the physics of polarization in a very elegant way. The first example of an approach along this line is presented in Sec. 7 for BeO, where the spontaneous polarization of Wurtzite *w*-BeO was evaluated using the zinc blende *zb*-BeO phase as a reference system with zero polarization.

An important point is that there must exist an adiabatic transformation of the system under consideration from the non-polar to the polar configuration, which keeps the solid insulating. For example, in the case discussed in Sec. 7, one can imagine the construction of a polar *w*-BeO phase from the infinite cubic non-polar *zb*-BeO crystal by generating a suitable sequence of stacking faults. A reference non-polar system may be also an artificial one: in the case of BN polar nanotubes, the non-polar nanotube consisted of artificial atoms that were 50% B and 50% N, and the built-up of polarization was followed by smoothly changing the properties of atoms (computing polarization many times along the way) until the nanotube become a real system with 100% B and N atoms [12].

The details of the theoretical approach are found in the papers by King-Smith and Vanderbilt [2] and by Resta [3]. Below, we outline only the main points. In quantum mechanics, all the information required for an unequivocal computation of polarization is contained in the system's wave functions. However, unlike the electron density $\rho(\vec{r})$, which is the squared *modulus* of the wave function, the polarization is fundamentally related to the *phase* of the wave function [2, 3]. Let's assume that the system is adiabatically transformed from a non-polar "reference" configuration to a polar one. During the transformation, an adiabatic current $\vec{j}$ must flow through the unit cell to account for the charge redistribution and the resulting polarization. The origin of this current, or more generally the intimate relationship of polarization with electric current, may intuitively be understood based on Fig. 1, which shows the piezoelectric effect. Initially, a crystal is unstrained and unpolarized. Application of strain induces both the distortion of the crystal and its polarization, which in turn is displayed by the presence of surface charge densities $\sigma$, due to electric currents that have flown through the crystal. This current may be measured when the crystal's surfaces are short-circuited, as shown in Fig. 1c. In a similar way, polarization

of *w*-BeO layers in a *w*-BeO/*zb*-BeO superlattice discussed in Sec. 7 and shown in Fig. 3 is related to the 2-dimensional charge densities accumulated at consecutive interfaces. These charge densities screen the polarization field present in the wurtzite part of the superlattice and can be viewed as the result of current flow created during an imaginary transformation of this part from a non-polar zinc-blende structure to the polar wurtzite structure.

Writing the complex wave functions as $|\psi(\vec{r})|\exp\{i\varphi(\vec{r})\}$, the current

$$\vec{j} = i(\psi\nabla\psi^* - \psi^*\nabla\psi) \tag{11}$$

will depend on the phases $\varphi(\vec{r})$ of system's wave functions. The geometric phase (or Berry phase) technique provides an elegant solution for the problem of computing electronic polarization in a periodic system by linking the phase evolution of the system's wave functions to the current flowing during the transformation and thus to the polarization change:

$$\Delta\vec{P}_{el} = \int_0^{\Delta t} \vec{j}(t)dt. \tag{12}$$

The ionic part of polarization $\vec{P}_{ion}$ is computed with a trivial summation over point charges of nuclei (or atomic cores).

More formally, let us assume that the system is adiabatically transformed from a non-polar reference configuration to a polar one. The transition may be parameterized with a variable $\lambda$, which changes respectively from 0 to 1. Resta [3] has proposed that the corresponding change in polarization is calculated using

$$\Delta\vec{P} = \int_0^1 (\partial\vec{P}/\partial\lambda)d\lambda \tag{13}$$

where within the LDA

$$\partial P_\alpha/\partial\lambda = \frac{ifq\hbar}{N\Omega m_e}\sum_k \sum_{n=1}^{M}\sum_{m=M+1}^{\infty} \frac{<\psi_{kn}^{(\lambda)}\left|\hat{p}_\alpha\right|\psi_{kn}^{(\lambda)}><\psi_{km}^{(\lambda)}\left|\partial V_{KS}^{(\lambda)}/\partial\lambda\right|\psi_{km}^{(\lambda)}>}{(\varepsilon_{kn}^{(\lambda)}-\varepsilon_{km}^{(\lambda)})^2} + c.c. \tag{14}$$

where $\alpha$ is the Cartesian direction, $V_{KS}$ is the self-consistent Kohn-Sham potential, $m_e$ is the electron mass, N is the number of the unit cells in the crystal, M is the number of the occupied bands, $\varepsilon_{kn}$ is the eigenenergy of the state $k$ in the $n$-th band, and $f$ is the occupation number of states in the valence band ($f = 2$ when spin degeneracy in taken into account).

After algebraic transformations described in detail in Ref. [2] one may obtain the electronic polarization per unit cell calculated from the periodic parts of the

occupied wave functions of the solid, $\psi_{nk}(\vec{r}) = u_{nk}(\vec{r})e^{i\vec{k}\vec{r}}$, as

$$\vec{P}_{el} = -\frac{2iq}{(2\pi)^3}\sum_{nocc}\int_{BZ} d\vec{k}\,\langle u_{nk}|\,\vec{\nabla}_k\,|u_{nk}\rangle\,. \tag{15}$$

If we denote by $\vec{G}_i$ the reciprocal lattice vectors defined by $\vec{G}_i \cdot \vec{R}_j = 2\pi m$, where $\vec{R}_j$ belongs to the real-space lattice of all allowable translations of the unit cell, we can introduce the electronic (or Berry) phase for the system as

$$\varphi_{el} = \Omega\vec{G}_i \cdot \vec{P}_{el}/q. \tag{16}$$

By following the change in the Berry phase during the transformation (which must keep the system insulating) we can obtain the difference in polarization. However, because the Berry phase (as a true angular variable) is calculated modulo $2\pi$, the polarization can only be obtained modulo $2q\vec{R}/\Omega$. The difference in total polarization, $\Delta\vec{P}$, will then be well defined if $|\Delta\vec{P}| << |2q\vec{R}/\Omega|$ or, if the change in the Berry phase is accurately monitored along a continuous path, as was done for the case of BN nanotubes, the multiple of $2q\vec{R}/\Omega$ in the Berry phase is also determined. This is important to ensure appropriate cancellation between the electronic and ionic terms, which can separately undergo large changes in their Berry phases [12].

Alternatively, one can transform the periodic wave functions into "bonding" functions, which tend to be localized around individual atoms or bonds in the unit cell. These are the so-called Wannier functions, which form an orthonormal basis and are defined as

$$W_n(\vec{r}) = V_{cell}/(2\pi)^3 \int \psi_{nk}(\vec{r})d\vec{k}, \tag{17}$$

where the integral is over the Brillouin Zone. The electron density is easily expressed in terms of Wannier functions

$$\rho(\vec{r}) = \frac{1}{(2\pi)^3}\sum_{nocc}\int |\psi_{nk}(\vec{r})|^2\, d\vec{k} = \sum_{nocc}|W_n(\vec{r})|^2. \tag{18}$$

The Wannier functions lead to an amazingly simple expression for polarization, namely

$$\vec{P}_{el} = -q\int \vec{r}\rho(\vec{r})d\vec{r} = -2q\sum_{nocc}\langle W_n|\,\vec{r}\,|W_n\rangle = -2q\sum_{nocc}\vec{r}_n, \tag{19}$$

which involves only the centers of Wannier functions $\vec{r}_n = \langle W_n|\,\vec{r}\,|W_n\rangle$. Thus, the difference in polarization, $\Delta\vec{P}$, is obtained by simply treating these centers as point charges that move during the transformation. No ambiguity arises, because the centers of the Wannier functions are uniquely assigned to each unit cell of the crystal. We may thus think of the electronic charge as being localized into point charges $-q$ located at the Wannier centers associated with the occupied states in each unit cell. In this picture, a quantum mechanical system of crystal electrons is mapped onto a

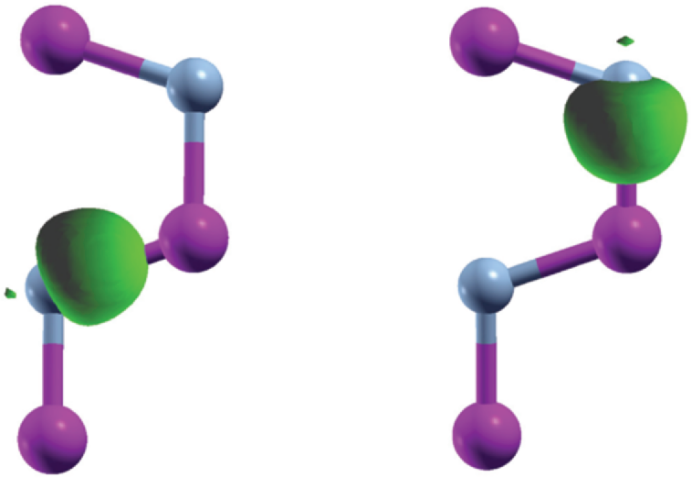

**Fig. 2** Examples of "$sp^3$" Wannier functions associated with the N atoms in AlN. Light and dark spheres represent N and Al atoms, respectively.

classical system of point charges, in analogy with the Clausius-Mossotti limit. As an example, in Fig. 2 we show two of the eight Wannier functions corresponding to the doubly occupied orbitals in the unit cell of *w*-GaN. Several algorithms have been developed to efficiently calculate Wannier functions [13, 14].

## 6 Polarization at Interfaces: Interface Dipoles

### *6.1 Averaging Microscopic Charges and Field*

The microscopic electric fields in solids, which are local and varying at length scales shorter than the lattice constant, are related to the microscopic charge density of nuclei and electrons by Poisson's equation. The electron density can be calculated from Schrödinger's equation or, when using density functional theory, from the self-consistent Kohn-Sham equations (9). However, in heterojunctions and other systems in which the effective mass description of the free carriers is valid, one is interested in macroscopic fields, which are slowly varying on the scale of a lattice constant.

To use Eqs. 1–5 on the macroscopic scale, it is convenient to average the electron density, the electrostatic potential, and the fields. In practice, the smallest possible and meaningful volume is that of the unit cell. In a heterojunction, the most convenient approach is to first average in the $(x,y)$ plane of the interface, and then average over an appropriate lattice period in the perpendicular direction. One should notice that the average electron density $n$ in Eqs. 1–5 is a macroscopic average of the microscopic charge density of valence electrons $\rho(\boldsymbol{r})$.

## 6.2 AlAs/GaAs Superlattice

To illustrate the conceptual aspects of linking macroscopic electrostatics with quantum-mechanical calculations, we summarize below the results of a study of electronic structure of interfaces in AlAs/GaAs superlattices [15], a simple but relevant example for the remainder of this chapter. The system studied was a (001)-oriented $(GaAs)_3(AlAs)_3$ superlattice consisting of three layers of each component. In the *zb* structure, the consecutive (001) planes contain only one kind of atoms. Their positions along the [001] axis are shown in the upper part of Fig. 3, and are denoted by Ga, Al, and As, respectively. The authors have used first-principles pseudopotential calculations and Fig. 3 also displays the average valence electron density $n$ and the electrostatic potential energy $V$ for this system.

We first analyze the electron density and begin with the obvious statement that the average electron density in bulk of a III-V compound is 8 electrons per unit cell. As is evident from the figure, in spite of the very short period of the superlattice, the calculated average electron density is 8 in the middle of each layer.

Next, conventional ideal interface planes of this system are placed on As atoms; one of them is in the middle of the figure, at $z = 0$, while the two others are at its edges. In the vicinity of interfaces the electron density differs from 8 by about 0.5 %. More precisely, across each interface the density has a typical dipolar shape and the sign of the dipoles alternates at consecutive interfaces. These results indicate that both the bulk region of each layer and interfaces between them are well defined. This, in turn, is necessary to correctly delineate the interfaces, and properly distinguish between bulk and interface effects. The calculated interface dipole layers, which have zero thickness in classical textbooks, turn out to extend over about 4 atomic monolayers, i.e., about 5 Å, in this particular case. This is indeed negligible in macroscopic samples. The dipoles are formed due to charge transfer between the nearest Ga-As and Al-As bonds only at the interface, which explains their strong spatial localization. Very similar results are found for (110)- and (111)-oriented superlattices [15].

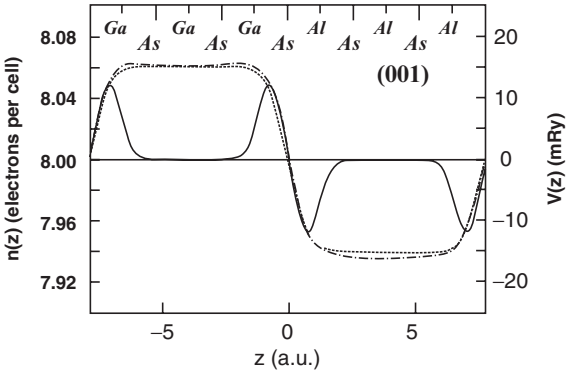


**Fig. 3** Macroscopic averages of electron density $n$ (full line) and potential energy $V$ (dashed-dotted line) of (001)-oriented $(GaAs)_3(AlAs)_3$ superlattice. See Ref. [15] for details. Figure reprinted with permission from Ref. [15]. Copyright (1988) by the American Physical Society.

In agreement with Eq. 4, the interface dipoles induce a difference in electrostatic energy, which is 0.41 eV. This energy is constant inside the GaAs and AlAs layers, which indicates that the electric field vanishes, as expected. It is the electrostatic contribution to the band offset in a GaAs/AlAs heterojunction.

## 7 Spontaneous Polarization in the Wurtzite Structure: BeO

The first calculations of spontaneous polarization in a crystal with the wurtzite symmetry, BeO, were performed by Posternak *et al*. [16]. They have used an infinite superlattice (SL) consisting of alternating layers of BeO in two phases, namely *w* and *zb*, shown in the upper panel of Fig. 4. The essential idea underlying this approach is that the *zb* phase has no intrinsic polarization due to its high symmetry, and thus the polarization in this system is entirely due to the spontaneous polarization of the wurtzite phase. Thus, the *zb* phase plays here the role of the non-polarized reference system, as mentioned earlier.

The results are shown in Fig. 4. The lower panel displays the averaged valence electron density and the potential energy. The average electron density *n* is practically constant in the middle of each layer and significant deviations from the average value only occur close to interfaces. Therefore, similar to the case of

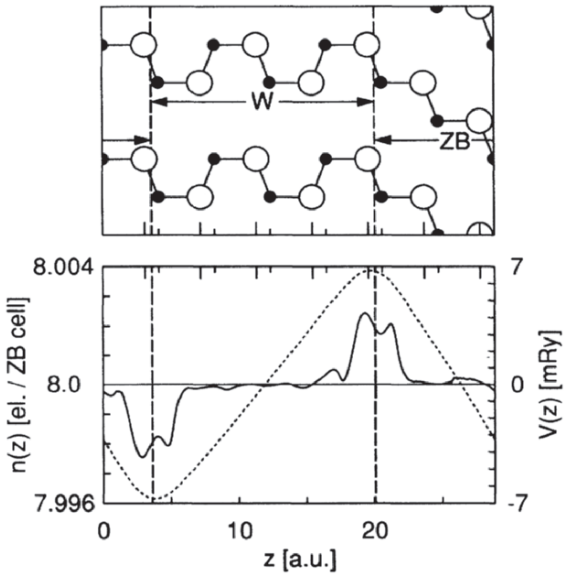


**Fig. 4** Upper panel: configuration of atoms in the large unit cell (i.e., one period of the SL). Solid and open circles represent Be and O atoms, respectively. With the usual conventions for the *w* structure, the positive *c*-axis direction points towards the right. Vertical dashed lines indicate the conventional interfaces between wurtzite and zinc blende layers. Lower panel: macroscopic averages of the electron density *n* (solid line) and of the electrostatic potential energy *V* (dotted line) in the case of ideal wurtzite geometry. Figure reprinted with permission from Ref. [16]. Copyright (1990) by the American Physical Society.

interface dipoles in GaAs/AsAs SL, interfacial monopoles are strongly localized and limited to about 2 monolayers, i.e., 4 Å. As expected, charge accumulation and depletion regions alternate at consecutive interfaces, generating an electrostatic potential via the Poisson's equation. Since the crystal is neutral, the formation of interface monopoles is due to charge transfer between interfaces and they have equal magnitudes and alternating signs.

Except for the regions at interfaces, the potential varies linearly in space, which corresponds to a constant electric field. Since polarization in the *zb* phase vanishes by symmetry, the polarization present in the system is entirely due to the layers of the wurtzite phase and has been calculated from the slope shown in Fig. 4. Finally, one should note the absence of interface dipoles, since at both sides of each interface there are the same Be-O bonds, and atoms in both *zb* and *w* structures have the same coordination of nearest neighbors.

The monopole contribution, i.e., the interface charge density, is related to the difference between bulk polarizations by the continuity equation, Eq. 4. In a general case, where *zb*-BeO and *w*-BeO layers are of different widths, Eq. 4 may be written in the form

$$\sigma_{\text{int}} = (P_A - P_B)(\iota_{\text{A}} + \iota_{\text{B}})/(\iota_{\text{A}}\,\varepsilon_{\text{B}} + \iota_{\text{B}}\,\varepsilon_{\text{A}}), \tag{20}$$

where $\iota$ is the width of a given layer, and $\varepsilon$ its static dielectric constant. In particular, when $\iota_{\text{A}} \neq \iota_{\text{B}}$ electric fields also differ.

As was mentioned earlier, the quantity of interest is the average electric field defined in Sec. 6 rather than the polarization. Electric fields are determined not only by the local charge distribution but also by the boundary conditions. A standard approach to compute the electronic structure of a semiconductor heterostructure is to use an appropriate superlattice. In this case, the use of periodic boundary conditions requires that the electrostatic potential is periodic, which results in electric fields in the two different parts of the superlattice having opposite signs, with a vanishing average over the full superlattice period. Moreover, the vanishing average electric field corresponds to short-circuiting of the two free surfaces in a finite sample.

We end this Section by mentioning that in the case of ideal *zb* and *w* layers of BeO shown in Fig. 4, the calculated electric field is $0.59 \times 10^9\,\text{V}/\text{m}$. It is also possible to determine the piezoelectric constant of *w*-BeO, by varying the geometry of atoms in the supercell from the ideal one to the appropriately distorted.

## 8 GaN/AlN Superlattice: Spontaneous Polarization and Piezoelectricity

The same approach has been used to study spontaneous polarization and piezoelectric effects in a GaN/AlN superlattice, in which both compounds have the wurtzite structure [17]. In this system, the two effects discussed above, i.e., the spontaneous polarization and the formation of interface dipoles, are simultaneously present. Moreover, in addition to the spontaneous polarization of GaN and AlN, there is a piezoelectric contribution to the polarization induced by the difference in lattice

constants of AlN and GaN, and the imposed assumption of pseudomorphic growth, i.e., the condition that the in-plane lattice constants of GaN and AlN are equal. The choice of the substrate (GaN, AlN, or an intermediate case) determines in which layer(s) the piezoelectric effect is present.

Figure 5 displays the atomic structure of the superlattice, the total average charge density (equal to zero in the bulk regions of every layer), and the macroscopic electrostatic potential. Qualitatively, these results can be viewed as a superposition of those from Figs. 3 and 4. First, the potential varies linearly within each layer, which demonstrates the presence of electric fields, and second, there are large 'discontinuities' at the interfaces that originate from formation of dipole layers via charge transfer between the nearest Al-N and Ga-N bonds at interfaces. It should be stressed that the electrostatic potential is continuous at the microscopic scale, and by a discontinuity $\Delta V$ we denote the difference between its averaged values at each side of the interface, as schematically shown in Fig. 5b.

These effects may be analyzed by decomposing the total charge density into a monopole and dipole components discussed in the previous examples. The results

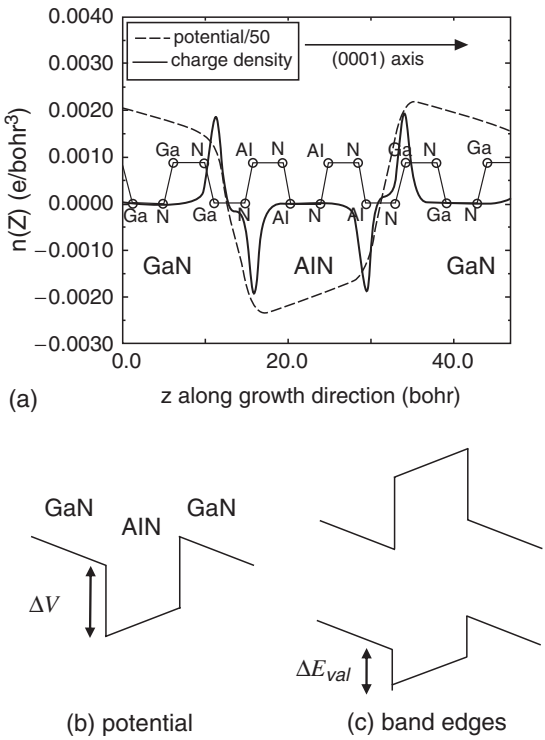


**Fig. 5** (a) Total (electronic plus ionic) density, and the electrostatic potential (in Hartrees), for AlN/GaN superlattice lattice-matched to GaN. The magnitude of the electric field is about $10^9$ V/cm. Note that the interfacial region is limited to about 5 Å. (Figure reprinted with permission from Ref. [17]. Copyright (1997) by the American Physical Society.) (b-c) Schematic of the potential energy shown in (a), and of the band offsets of GaN/AlN superlattice.

are shown in Fig. 6. While an exact definition of the monopole and dipole contributions is not possible in the low-symmetry wurtzite lattice, which in particular lacks an inversion plane perpendicular to the *c*-axis, the procedure used by the authors is satisfactorily accurate, see [17] for details.

The monopole component gives rise to macroscopic electric fields and is due to both the spontaneous polarization and the piezoelectric effects. In principle, it can be calculated *a la* Posternak *et al*. [16] separately for GaN and AlN using appropriate superlattices. However, it is the difference of polarizations between GaN and AlN, and between the generated electrostatic fields, which is of practical importance. The calculated fields are about $10^9\,\mathrm{V/m}$, similarly to those in BeO.

For obtaining the full spectrum of polar properties, it is easier and more accurate to use the Berry phase approach. The values of the spontaneous polarization $P_{eq}$, effective charge $Z$, and the two components of the piezoelectric tensor calculated using this method are given in Table 1. Similar values were obtained in Ref. [18]. For comparison, the results for ZnO are also presented.

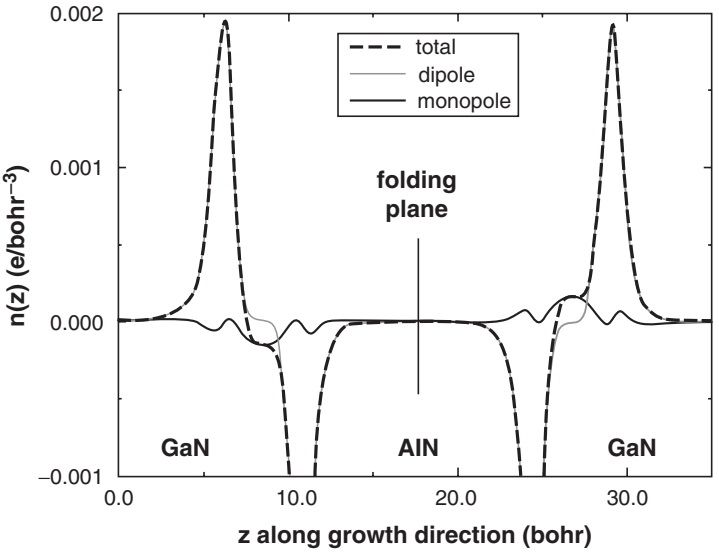


**Fig. 6** Total electron density (dash-dotted), and its monopole (solid) and dipole (dashed) components for the superlattice shown in Fig. 5. Figure reprinted with permission from Ref. [17]. Copyright (1997) by the American Physical Society.

**Table 1** Spontaneous polarization $P_{eq}$, (in $\mathrm{C/m^2}$) effective charge $Z^*$, and the two components of the piezoelectric tensor (in $\mathrm{C/m^2}$) calculated in Ref. [19].

| | $P_{eq}$ | $Z^*$ | $e_{33}$ | $e_{31}$ |
|---|---|---|---|---|
| AlN | −0.081 | −2.70 | 1.46 | −0.60 |
| GaN | −0.029 | −2.72 | 0.73 | −0.49 |
| InN | −0.032 | −3.02 | 0.97 | −0.57 |
| ZnO | −0.057 | −2.11 | 0.89 | −0.51 |

Given the similarity of the [0001] direction in wurtzite with the [111] direction in zinc-blende crystals, it is possible and meaningful to compare the respective components of the piezoelectric tensor of the nitrides with those of other *zb*-III-V and *zb*-II-VI semiconductors. The detailed results of Ref. [19] show that:

(i) The absolute values of the piezoelectric constants are an order of magnitude higher in group-III nitride crystals than in other III-V and II-VI crystals.
(ii) Similarly, the spontaneous polarization is very large and only about 4 times smaller than in typical perovskite ferroelectric crystals.
(iii) The sign of the piezoelectric constants is the same as in II-VI compounds but opposite to the III-V ones. This effect is due to the high ionicity of III-N nitrides, as manifested by the high values of the effective charges $Z$, which are close to those of ZnO (see Table 1), and higher than those of phosphides or arsenides. Consequently, the internal-strain ionic contribution, which is proportional to $Z$, dominates the clamped-ion term in Eq. 8.
(iv) Among the nitrides, the spontaneous polarization of AlN is the strongest because of its largest deviation from the ideal wurtzite structural parameters ($c/a = \sqrt{8/3}$, and $u = 0.375$).

Finally, for application purposes, alloys with tailored chemical compositions are often of greater interest than pure binary compounds. For this reason, the important physical properties of III-N alloys, like GaInN, have been investigated as a function of chemical composition. The obtained results show that lattice parameters follow Vegard's law, i.e., they change linearly with composition. On the other hand, polarization in III-N alloys turns out to be a non-linear function of the chemical composition of the alloy [18, 20, 21]. This holds for both the spontaneous polarization and the piezoelectric constants. The main reason for these non-linear dependences is the lattice mismatch, i.e., the difference between the lattice constants of the nitrides, which results in internal distortions in alloys.

As in the case of GaAs/AlAs superlattices, potential discontinuities contribute to band energy discontinuities or band energy offsets at heterointerfaces, as shown in Fig. 5c. The offsets are found to depend on the substrate: for AlN on GaN $\Delta E_{val} = 0.20\,\text{eV}$, and for GaN on AlN $\Delta E_{val} = 0.85\,\text{eV}$ [17]. The non-equivalence of the two cases is strain-induced, caused by strong piezoelectricity of the nitrides. Similar results were obtained by Buongiorno Nardelli *et al*. [22] for zinc-blende GaN/AlN superlattices.

# 9 Electric Field-Driven Diffusion and Segregation of Dopants in Superlattices

## *9.1 Introduction*

Polarization in bulk III-N nitrides results in the presence of electric fields discussed in the previous Sections. The impact of these fields on the electronic properties has

been briefly mentioned above and is discussed in detail in several chapters of this book. The aim of this Section is to point out that electric fields, if strong enough, alter not only the electronic structure, but also the distribution of dopants and defects in nitride-based quantum structures. They may also result in electrodiffusion of charged dopants.

Hydrogen in GaN/AlN superlattices is chosen as the key example; it is the dominant impurity that passivates dopants in structures grown by metalorganic chemical vapor deposition. As will be shown below, the distribution of H in a GaN/AlN superlattice is determined not only by its solubility, but also by the presence of electric fields. We show that these fields give rise to a field-driven electrodiffusion of charged impurities, which can lead to, e.g., an accumulation of hydrogen close to the appropriate interfaces.

In general, properties of semiconductor structures rely entirely on accurate control of doping and stoichiometry. These, in turn, are determined by solubility of impurities and the presence of native defects. For this reason, the issue of equilibrium concentrations of dopants and defects in bulk semiconductors has been extensively studied in the last decade. The first principles theory of doping efficiency [23, 24] allows one to relate the equilibrium concentrations of dopants with the conditions of crystal growth. Moreover, in the wide-gap III-N nitrides self-compensation, i.e., non-intentional formation of native defects, plays an important role [25]. However, since semiconductor systems of current interest are not *bulk* materials but rather *epitaxial heterostructures*, such as GaN/AlN, a question arises about the equilibrium distribution of dopants and defects in heterostructures. Experimentally, thermally activated segregation of impurities through semiconductor heterointerfaces has been investigated for Si/SiGe heterostructures, where the equilibrium concentrations of dopants in Si and SiGe layers differ by a factor of two to three [26–29]. The segregation is stronger in III-V heterostructures [28, 30, 31], where concentration differences may reach two orders of magnitude and affect the luminescence efficiency of light-emitting diodes [32]. A theory of interfacial segregation has been recently formulated in modern terms [33], allowing studies of this effect by accurate *ab initio* methods.

To illustrate the general features that determine segregation, typical dopants and defects in GaN/AlN structures are discussed. The results show that the distribution of dopants in a heterojunction cannot in general be obtained from calculations performed for isolated bulk crystals. The large differences in segregation properties between cation- and anion-substituting dopants are discussed and explained, as are those between shallow and deep ones, and the impact of the defect's charge state (the Fermi level position) on segregation.

## *9.2 Interfacial Segregation*

Consider first the basic concepts describing the doping of a homogeneous solid: The equilibrium concentration of dopants is defined for given conditions of growth under

the assumption that equilibrium is maintained between the growing sample and the reservoirs of relevant atomic species characterized by their chemical potentials μ [23, 24]. At these conditions, insertion of an impurity atom into a solid induces a change in the total energy of the system, which is the formation energy $E_{form}$. For example, $E_{form}$ of a neutral interstitial H in GaN is

$$E_{form} = E_{tot}(\mathrm{GaN:H}) - E_{tot}(\mathrm{GaN}) - \mu(\mathrm{H}), \tag{21}$$

where $E_{tot}$ is the total energy of the crystal with or without the impurity. Neglecting small changes in the vibrational entropy, one finds that the equilibrium concentration of dopants is equal to

$$N_{imp} = N_0 \exp(-E_{form}/k_{\mathrm{B}}T), \tag{22}$$

where $N_0$ is the density of lattice sites that can be occupied by a given dopant.

Turning to interfacial segregation in an A/B heterostructure, the equilibrium concentrations of dopants at the A and B components, $N_{imp}(\mathrm{A})$ and $N_{imp}(\mathrm{B})$ respectively, are determined by the condition that the chemical potential of the dopant is the same in the whole system, and in particular at both sides of the interface. Using this fact one finds that the segregation coefficient, defined as the ratio of impurity concentrations at the two sides of the interface, is

$$k_{seg} = N_{imp}(\mathrm{A})/N_{imp}(\mathrm{B}) = N_0(\mathrm{A})/N_0(\mathrm{B}) \exp(E_{seg}/k_{\mathrm{B}}T), \tag{23}$$

where $E_{seg} = E_{form}$ (A) - $E_{form}$ (B) is the segregation energy. Therefore, $k_{seg}$ only depends on the difference between the formation energies and is independent of $\mu_{\mathrm{imp}}$, i.e., of the actual source of the impurity atoms. To describe quantitatively the interfacial segregation, the above analysis needs to be supplemented by first principles calculations of the total energies. They were done using the methods described in Sec. 4.

In general, dopants and defects in semiconductors are ionized. Ionization of dopants affects their distribution in GaN/AlN heterojunctions in two ways that are discussed in more detail below. First, electric fields present in a junction lead to field-driven diffusion and redistribution of ionized dopants. This effect was seen experimentally for B in a Si homojunction [34]. Second, in a homogeneous crystal, $E_{form}$ depends on the charge state of the defect. The transfer of $m$ electrons from a defect level $E_{imp}$ to the Fermi level $E_F$ changes the formation energy by $m(E_F - E_{imp})$, which should be added to the right-hand side of Eq. 21 [23, 24]. Consequently, since $E_{seg}$ is the difference between $E_{form}$ of the two materials, segregation depends on the charge state of the defect as well. It will be shown below that this dependence is in general weak for shallow defects, but may be substantial for deep ones.